Mixed quantum-classical treatment of reactions at surfaces with electronic transitions

Christian Bach, Christian Carbogno and Axel Groß
Physik-Department T30, Technische Universität München, D-85747 Garching, Germany
(Dated: April 30, 2004)

The reliable high-dimensional theoretical description of reactions at surfaces with electronic transitions still represents a considerable challenge since the electrons have to be treated quantum mechanically. A full quantum treatment of both electrons and nuclei is computationally not feasible at the moment. Therefore we propose a mixed quantum-classical approach for the simulation of reactions at surfaces with electronic transitions. In this method, the nuclear motion is described classically while the electrons are treated quantum mechanically. Still the feedback between nuclei and electrons is taken into account self-consistently. The computational efficiency of this method allows a more realistic multi-dimensional treatment of electronically non-adiabatic processes at surfaces. We will discuss two recent applications of this approach. First we will address the charge transfer in the scattering of I_2 from a diamond surface. As a second example we present dynamical simulations of the laser induced desorption of NO from NiO(100).

Keywords: Ab initio quantum chemical methods and calculations, semi-empirical models and model calculations, atomistic dynamics, molecule-solid scattering, charge transfer, desorption induced by electronic transitions (DIET)

I. INTRODUCTION

There is a wide variety of processes at surfaces that involve electronic transitions. Electronically non-adiabatic reactions such as, e.g., charge transfer processes [1], exoelectron emission [2] or electron-hole pair excitations in the substrate [3] might be caused by the interaction of atoms and molecules with surfaces. Or alternatively, surface processes might be triggered either by photons or electrons incident of a surface, a prominent example being desorption induced by electronic transitions (DIET) [4–6]. Experimentally, such processes have been studied extensively in recent years. Technological progress has made it possible to perform time-resolved laser pump-probe experiments in which the time evolution of electronically non-adiabatic reactions can be monitored in the femtosecond regime [7, 8]. These experiments provide a wealth of information on the real-time dynamics of chemical processes at surfaces [9, 10].

Unfortunately, the development of theoretical tools for the realistic description of electronically non-adiabatic processes did not match the experimental progress. The main reason for this is the fact that the modelling of processes involving several electronic states and transitions between them still represents a great challenge. First of all, for the ab initio determination of excited state potentials it is not possible to use the computational efficient density-functional theory schemes which work so well for the ground state. Instead one has to rely on quantum chemistry methods which are usually computationally very costly. And second, the simulation of the dynamics of electronically non-adiabatic processes explicitly requires the simultaneous treatment of both the electronic and the nuclear dynamics. There has been significant progress in the high-dimensional simulation of Born-Oppenheimer reaction dynamics at surfaces in recent years [11–16]. These studies in fact demonstrated the importance of the multidimensionality in the reaction dynamics. However, electronically non-adiabatic simulations of reactions at surfaces are usually limited to a few degrees of freedom [17]. This is caused by the difficulties in the theoretical treatment due to the different time scales relevant for the electronic and nuclear motion.

To allow a multidimensional treatment of reactions with electronic transitions, we have proposed the use of mixed quantum-classical schemes in which the nuclear motion is described classically while at the same time the electrons are treated quantum mechanically [18–22]. Still the feedback between quantum and classical degrees of freedom has to be taken into account in a self-consistent way. The mixed quantum-classical scheme we have used is based on the fewest switches algorithm developed by Tully [18]. This surface-hopping algorithm minimises the number of state switches under the constraint of maintaining the correct statistical population of each electronic state, as given by the quantum mechanical part of the system.

Here we will first give a rather extended introduction into the theory underlying the surface-hopping method we have been using. Then we will review our recent applications of this mixed quantum-classical scheme to the simulation of electronically non-adiabatic processes on surfaces, but we will also present some new results. The first system addressed is the charge transfer in the scattering of iodine from a diamond surface. We propose that it is not the electronic coupling *per se* that determines the ionization probability of I_2 as a function of the kinetic energy but rather the energy transfer into other degrees of freedom during the scattering event. We will also present new findings addressing the preservation of the quantum coherence in the mixed quantum-classical calculations.

The second process we will discuss belongs to the class of the photo-induced desorption of simple molecules from surfaces. We have performed high-dimensional simulations of the laser induced desorption of NO from

NiO(100). The potential energy surface (PES) used was based on a low-dimensional *ab initio* PES [23] that we have extended in order to include all molecular degrees of freedom plus one surface oscillator coordinate. In order to include the effect of electronic substrate states, we have introduced an optical potential in the mixed quantum-classical algorithms. We will show that by considering more degrees of freedom certain aspects of the experimental situation are better reproduced, but others are not. In addition, we show new results including a more realistic description of dissipation effects in the desorption dynamics. These two examples illustrate that the mixed quantum-classical method allows a more realistic multi-dimensional treatment of electronically non-adiabatic processes at surfaces.

II. THEORY

In this section, we will review the theoretical foundations of mixed quantum-classical surface hopping methods. Our presentation is mainly based on Refs. [24] and [25]. Then we will briefly describe the fewest switches algorithm [18] and its extension including an optical potential [21, 22].

In order to simulate the dynamics of electronically non-adiabatic processes, all relevant nuclear coordinates, electronic states and the coupling between these states have to be taken into account. For an approximate treatment, the first step is a separation between slow and fast coordinates, denoted by r and R, respectively. The fast degrees of freedom, usually the electrons, will require explicit quantum mechanical treatment. The dynamics of the slow coordinates can be treated with quantum mechanical methods but in most cases a classical treatment will be sufficient. We will use the term electronic coordinates as a synonym for the fast degrees of freedom, despite the fact that those might include some proton positions as well [26, 27]. Correspondingly we will use the term nuclear coordinates for the slow degrees of freedom.

The Hamilton operator of a system that separates into slow and fast degrees of freedom can be written in the following form

$$H(r,R) = T_R + T_r + V(r,R), \tag{1}$$

where V is the potential and T_R and T_r are the kinetic energy operators for the slow degrees of freedom and for the electronic coordinates, respectively. The potential can be split further into three parts

$$V(r,R) = V_{rr}(r) + V_{RR}(R) + V_{rR}(r,R), \tag{2}$$

the interaction of the electrons with each other $V_{rr}(r)$ the interaction between the nuclei $V_{RR}(R)$ and the interaction of the nuclei with the electrons $V_{rR}(r,R)$.

The dynamics of the system is given by the solution of the time dependent Schrödinger equation

$$i\hbar\frac{\partial}{\partial t}\Psi(r,R,t) = H\Psi(r,R,t). \tag{3}$$

In surface hopping, the wave function is expanded in an orthonormal basis set of electronic wave functions $\phi_i(r,R)$

$$\Psi(r,R,t) = \sum_i \psi_i(R,t)\phi_i(r,R) \tag{4}$$

where the nuclear position R acts as a parameter. Insertion into the Schrödinger equation (3), multiplication with $\phi_j^\star$ from the left and integration over r leads to a set of coupled equations for the ψ_i's:

$$\begin{aligned} i\hbar\dot{\psi}_j(R,t) &= (T_R + V_{RR})\,\psi_j(R,t) \\ &+ \sum_i \left[V_{ji} - \sum_{\alpha=1}^{3N} \frac{\hbar^2}{2M_\alpha} D_{ji}^\alpha + \sum_{\alpha=1}^{3N} \frac{i\hbar}{M_\alpha} d_{ji}^\alpha \left(i\hbar\nabla_{R_\alpha}\right)\right] \psi_i(R,t) \end{aligned} \tag{5}$$

where N is the number of nuclei and M_α the mass corresponding to the α-th coordinate R_α. Here we have introduced the non-adiabatic coupling vectors $D_{ji}^\alpha(R)$ and $d_{ji}^\alpha(R)$ as

$$D_{ji}^\alpha(R) = \langle\phi_j(r,R)|\nabla_{R_\alpha}^2|\phi_i(r,R)\rangle \tag{6}$$

and

$$d_{ji}^\alpha(R) = \langle\phi_j(r,R)|\nabla_{R_\alpha}|\phi_i(r,R)\rangle, \tag{7}$$

now making use of the bra-ket notation with integration over the fast coordinates r only. The matrix elements $V_{ji}(R)$ of the electronic Hamiltonian H_r are given by

$$V_{ji}(R) = \langle\phi_j(r,R)|H_r(r,R)|\phi_i(r,R)\rangle, \tag{8}$$

where H_r is the electronic Hamiltonian

$$H_r(r,R) = T_r + V_{rr}(r) + V_{rR}(r,R). \tag{9}$$

For notational convenience we will later drop the summation over α as an index of the coordinates. Now we take the classical limit for the nuclear part of the wave function by splitting $\psi_i(R,t)$ into an amplitude $A_i(R,t)$ and a phase $S_i(R,t)$:

$$\psi_i(R,t) = A_i(R,t)e^{\frac{i}{\hbar}S_i(R,t)}. \tag{10}$$

If we insert eq. (10) into eq. (5), multiply with $e^{-\frac{i}{\hbar}S_i(R,t)}$ and take the classical limit $\hbar \to 0$, we obtain a separate equation for each index j of the form

$$\dot{S}_j + \frac{1}{2M}\left(\nabla_R S_j\right)^2 + V_{jj}(R) + V_{RR}(R) = 0. \tag{11}$$

This is just the Hamilton-Jacobi equation

$$H_j\left(R, \frac{\partial S_j}{\partial R}\right) + \frac{\partial S_j}{\partial t} = 0 \tag{12}$$

with an Hamilton function for each state ϕ_j

$$H_j(R,P) = \frac{1}{2M}P^2 + V_{jj}(R) + V_{RR}(R). \tag{13}$$

The equations of motion governing the classical particles are then given by

$$M_\alpha \ddot{R}_\alpha(t) = -\nabla_{R_\alpha}\left[V_{jj}(R) + V_{RR}(R)\right]. \quad (14)$$

The motion of the nuclei along a trajectory $R(t)$ is at any time t given by the forces between the classical particles $-\nabla_R V_{RR}$ and the potential V_{jj} of a single state ϕ_j.

There are some liberties in how to implement the hopping between the potential energy surfaces resulting in various surface hopping versions. For example, in their original paper Tully and Preston allowed jumps only at distinct points in configuration space, namely at the crossings of the diabatic potentials [28]. This has the advantage of eliminating the need to adjust the kinetic energy during a hop, but determining the crossing lines of higher dimensional energy surfaces can be a difficult problem to solve. In contrast to that, the fewest switches algorithm, introduced by Tully in Ref. [18], allows switches at any position but requires some form of energy adjustment to recover energy conservation.

In this work we will focus on the fewest switching algorithm. The electronic wave function $\phi(r,t)$ is expanded in a set of orthonormal basis functions $\phi_i(r,R)$ with a parametric dependence on the nuclear coordinates and coefficients $c_i(t)$

$$\phi(r,t) = \sum_i c_i(t)\,\phi_i(r,R(t)). \quad (15)$$

In order to determine the time evolution of the coefficients c_j, one considers $\frac{\partial}{\partial t} A_j^\star A_j$ and identifies c_j with $A_j e^{\frac{i}{\hbar}S_j}$. Then the time evolution of the coefficients is given by [24, 25]

$$\begin{aligned}\dot{c}_i(t) &= -\sum_j \left\{ c_j(t) \sum_\alpha \left[\dot{R}_\alpha(t) d_{ij}^\alpha\left(R(t)\right)\right]\right\} \\ &\quad -\frac{i}{\hbar}\sum_j V_{ij}\left(R(t)\right) c_j(t). \end{aligned} \quad (16)$$

We now can define the components of the density matrix $a_{ij} \equiv c_i^\star c_j$ with the diagonal elements being the occupation probabilities of the corresponding states. The time derivative of the a_{ij} is given by

$$i\hbar\dot{a}_{kj} = \sum_l \{a_{lj}[V_{kl} - i\hbar\dot{\vec{R}}\vec{d_{kl}}]\} - a_{kl}[V_{lj} - i\hbar\dot{\vec{R}}\vec{d_{lj}}]\}\,. \quad (17)$$

For the diagonal elements a_{ii}, this equation can be simplified to

$$\dot{a}_{ii} = \sum_j b_{ij} \quad (18)$$

where the b_{ij} are defined as

$$b_{ij} = \frac{2}{\hbar}\Im\left[a_{ij}V_{ij}\right] - 2\Re\left[a_{ij}d_{ij}\dot{R}\right]. \quad (19)$$

Note that the b_{ij} are anti-symmetric under index interchange $b_{ij} = -b_{ji}$ following from the fact that the d_{ij} are anti-symmetric as well.

At any given time the system is considered to be in a single basis state, the currently occupied state, which we will denote with ϕ_{occ}. The motion of the slow degrees of freedom is governed by that state

$$\begin{aligned}\ddot{R}_\alpha(t) &= \frac{-1}{M_\alpha}\nabla_{R_\alpha}\left\{V_{RR}\left(R(t)\right)\right. \\ &\quad \left. + \int dr\ \phi^\star_{occ}\left(r,R(t)\right) H_r\left(r,R(t)\right)\phi_{occ}\left(r,R(t)\right)\right\} \end{aligned} (20)$$

Note that this set of equations was derived, in a slightly different manner, by Tully in Ref. [18] with the assumption that the slow particle movement is given by a trajectory and that the electronic wave function is expanded according to eq. (15).

One problem with the mixed quantum classical surface hopping is the dependence on the choice of basis functions. Usually we will use the adiabatic basis, but depending on the particular system it is not always clear what would be an optimal basis [20].

We will now discuss how the occupied state is determined in the fewest switches algorithm. The equations (16) and (14) are integrated simultaneously and, between integration steps, switches between the electronic states are performed, in order to maintain the correct statistical occupation probabilities. This method minimises the number of switches performed. How this is achieved is explained nicely in [18] and we will follow that presentation. If we consider a swarm of N trajectories with occupation probabilities a_{ii} at time t and a'_{ii} at time $t' = t + \Delta t$ then $N_i = a_{ii}N$ and $N'_i = a'_{ii}N$ are the number of trajectories in state i at times t and $t + \Delta t$. The net change of the number of trajectories in state i is then given by

$$\Delta N_i = N'_i - N_i = \left(a'_{ii} - a_{ii}\right)N. \quad (21)$$

For short time steps Δt we can replace the difference $a'_{ii} - a_{ii}$ with $\dot{a}_{ii}\Delta t$ and using eq. (18) we get

$$\Delta N_i = \dot{a}_{ii}\Delta t N = N\Delta t \sum_j b_{ij}, \quad (22)$$

with the state-to-state transition rates b_{ij} giving the change in state i due to state j, as defined in eq. (19). Thus only if b_{ij} is less than zero trajectories jump from state i into state j and their number is given by $N\Delta t b_{ji}$. If we now divide that by the number of trajectories in state i we get the probability p_{ij} for a trajectory to jump from state i into state j

$$p_{ij} = \frac{N\Delta t b_{ji}}{a_{ii}N} = \Delta t \frac{b_{ji}}{a_{ii}}. \quad (23)$$

Note that the switching probabilities are proportional to the time step, thus the total switching probability for a trajectory when passing through a certain region is, apart from an discretisation error, independent of the time steps used. Note also that the probabilities given by eq. (23) could in principle get arbitrarily large, but usually the time step required for accurate integration of eq. (16) is small and switches will be improbable (see also Ref. [19]).

The procedure for the simulation of a single surface hopping trajectory with the fewest switching method can be roughly divided into the following five steps.

Step 1 Set initial conditions for the nuclear coordinates R and velocities $\dot{R}$, the coefficients of the electronic states c_i and choose the currently occupied state.

Step 2 Integrate eq. (16) and eq. (14) for the time step Δt with the currently occupied state j.

Step 3 According to eq. (23), determine the switching probabilities from the current state to all other states. Calculate the p_{ji}'s and set all with $p_{ji} < 0$ to zero (fewest switches). Draw a uniformly distributed random number z in the range of $0 < z < 1$. Jump into the state i for which $\sum_{l=1}^{i-1} p_{jl} < z \leq \sum_{l=1}^{j} p_{jl}$.

Step 4 If a switch to the state l occurs, usually the potential energies $V_{jj}(R)$ and $V_{ll}(R)$ differ at the current position R. To recover energy conservation the velocity is adjusted accordingly in the direction of the non-adiabatic coupling vector $d_{jl}(R)$, for justification of this particular choice see references [29–31]. If the kinetic energy is not sufficient to cover the potential energy difference the hop is refused and propagation continues on the original potential energy surface.

Step 5 Repeat steps two to four until the trajectory satisfies an appropriate stopping condition.

There are some problems with the surface hopping approach that shall be briefly mentioned here. While the trajectory stays in one state the total energy of the system is clearly conserved. But one problem is how to retain energy conservation upon a jump between surfaces with different potential energies. As mentioned above there are some arguments, derived from semiclassical considerations by Pechukas in [32, 33], to adjust the velocity along the non-adiabatic coupling vector in order to compensate for the difference in potential energy. This requires the solution of the following equation

$$0 = \Delta V + \lambda \sum_\alpha \frac{\dot{R}_\alpha d_{ij}^\alpha}{M_\alpha} + \lambda^2 \sum_\alpha \frac{{d_{ij}^\alpha}^2}{M_\alpha}, \tag{24}$$

where ΔV is the change in potential energy and the new velocity is given by $\dot{R}_{new} = \dot{R}_{old} + \lambda d_{ij}$ (for a graphical representation see Fig. 1). Usually this equation has two solutions λ and it is not clear which one should be

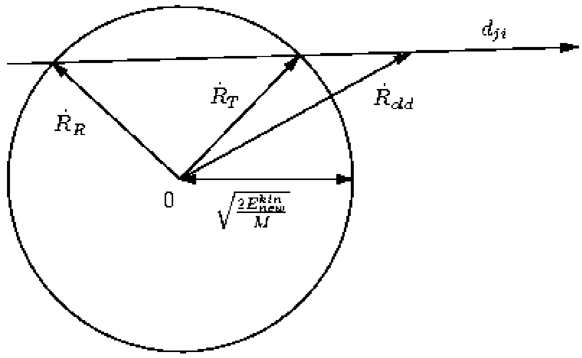

FIG. 1: Schematic drawing of the rescaling of the velocity in two dimensions after an switch occurred. $\dot{R}_{old}$ is the velocity before the hop and $\dot{R}_T$ and $\dot{R}_R$ are the two new velocities corresponding to the two solutions for λ of 24. The radius of the circle is given by the velocity after the jump, where E_{new}^{kin} is the new kinetic energy.

used. The solution with the smaller absolute value corresponds to a transmission of the surface normal to d_{ij} and the solution with the larger value is a reflection. As is suggested in [31, 34] we used the λ with the smaller absolute value. This corresponds to the suppression of any quantum reflection at the position of the switch.

Another problem is that quantum mechanics allows the intrusion of the wave function into classical forbidden areas. This results in hops where there is no solution for eq. (24). In the case of such an event one has to either sacrifice consistency, suggesting a hop, or energy conservation. In the fewest switches algorithm energy forbidden hops are rejected thus partially giving up consistency. There is an extensive discussion in the literature about this problem, but to our knowledge no satisfactory solution has been found yet [35, 36].

Recently, a combination of the surface hopping and the mean field methods was proposed [37]. In this method the nuclear degrees of freedom evolve along a classical trajectory $R(t)$ and the electronic wave function is only partially expanded in a finite set of S orthonormal functions ϕ_i and the remainder of the wave function ϕ_C is treated collectively

$$\phi(r,t) = \sum_{i=1}^{S} c_i(t)\phi_i\left(r, R(t)\right) + \phi_C\left(r, R(t)\right). \tag{25}$$

The equation of motion for ϕ is given by

$$i\hbar\frac{\partial}{\partial t}\phi(r,t) = H_r\left(r, R(t)\right)\phi(r,t), \tag{26}$$

which is a time dependent Schrödinger equation due to the time dependence of $R(t)$. The electronic Hamiltonian H_r was defined before in eq. (9). The occupied state ϕ_{occ} can now be either one of the ϕ_i or the collective state ϕ_C. Since the collective state ϕ_C is not necessarily normalised, the equations of motion for the slow particles become

$$\ddot{R}_\alpha(t) = \frac{-1}{M_\alpha} \nabla_{R_\alpha} \left[V_{RR}\left(R(t)\right) + \frac{\int dr\ \phi^\star_{occ}\left(r, R(t)\right) H_r\left(r, R(t)\right) \phi_{occ}\left(r, R(t)\right)}{\int dr\ \phi^\star_{occ}\left(r, R(t)\right) \phi_{occ}\left(r, R(t)\right)} \right] \quad (27)$$

The time evolution of the system is given by equations (26) and (27) and for the occupation probabilities we get

$$\dot{a}_{ii} = \sum_{j=1}^{S} b_{ij} + b_{iC}, \quad (28)$$

with the b_{ij} as in eq. (19) and b_{iC} defined as

$$b_{iC} = \frac{2}{\hbar} \Im\left[c_i^\star V_{iC}\right] - 2\Re\left[c_i^\star \langle \phi_i | \dot{\phi}_C \rangle\right]. \quad (29)$$

The population $a_{CC} \equiv \langle \phi_C | \phi_C \rangle$ in the collective state is computed using the normalisation of the electronic wavefunction, and for the time derivative we get

$$\dot{a}_{CC} = -\sum_{i=1}^{S} \dot{a}_{ii} = -\sum_{i=1}^{S} b_{iC}. \quad (30)$$

For the second expression we used eq. (28) and the fact that the b_{ij} are anti-symmetric under index interchange. Note that the generalised surface hopping contains mean field, if $S = 0$, as well as the "classical" surface hopping, if $\phi_C = 0$.

A large drawback of this method is the need for explicit propagation of the wave function according to eq. (26). This is usually a much more demanding task than the integration of equation 16 since it requires an additional evaluation of the kinetic energy operator.

We have adopted the generalised surface hopping algorithm in order to address laser-induced reactions at surfaces combining ideas of previous treatments [18, 37–39]. In particular, we have introduced an optical potential in order to simulate the collective influence of electronic excitations of the substrate. The resulting mixed quantum classical method will allow the inclusion of all the relevant nuclear coordinates of both adsorbate and substrate at sufficiently long propagation times to correctly describe thermalization and dissipation effects.

One of the problems encountered when modelling DIET processes with surface hopping algorithms is the huge number of electronic adsorbate and substrate states involved which need to be taken into account. Due to the large number of and similar shapes of the corresponding potentials, it is clear that it is neither feasible to explicitly include all these substrate states into our simulation nor is it necessary since the reaction dynamics is dominated by a few adsorbate states, which must be taken into account. The main effect of the substrate states is coupling different adsorbate states either to each other or to an external electromagnetic field. We model this effect collectively by combining ideas from Tully's fewest switching algorithm [18] and generalised surface hopping method [37] with those of Brenig [38] and Saalfrank [39] who introduced optical potentials to the description of DIET processes.

As with all methods before the Hamiltonian H is split into the kinetic energy T_R of the nuclear coordinates R and an electronic part H_r, where the electronic part depends explicitly on the electronic coordinates r and parametrically on the position of the nuclei R

$$H(r, R) = T_R + H_r(r, R). \quad (31)$$

Just as in the generalised surface hopping algorithm, the electronic wave function Ψ is expanded into the explicitly treated excited adsorbate states ϕ_i and a collective state ψ containing the molecular ground state together with the continuum of substrate excitations

$$\Psi(r, R, t) = \sum_i c_i(t) \phi_i(r, R) + \phi_C(r, R, t). \quad (32)$$

The influence of this collective state ϕ_C on the rest of the electronic system can be taken into account by an effective non-Hermitian Hamiltonian (see chapter 16 in [40])

$$H_{eff}(r, R) = T_r + V_{eff}(r, R) + i\Delta(r, R), \quad (33)$$

where T_r is the kinetic energy operator of the electrons. The effective potential V_{eff} and the optical potential Δ are real functions of r and R. In a Newns-Andersson picture Δ is related to the lifetime broadening of a resonance state which can be determined via [41]

$$\Delta(E) \;=\; \pi \sum_{\mathbf{k}} |V_{\mathbf{k}}|^2 \delta(E - \varepsilon_{\mathbf{k}}). \quad (34)$$

With the effective Hamiltonian and a diabatic (i.e. $\nabla_R \phi_i = 0$) representation of the wave functions ϕ_i, the electronic Schrödinger equation has the following form

$$\dot{c}_j = -\frac{i}{\hbar} \sum_i c_i V_{ji} + \frac{1}{\hbar} \sum_i c_i \Delta_{ji}, \quad (35)$$

where the matrix elements V_{ij} and Δ_{ji} are defined as

$$\begin{aligned} V_{ji} &\equiv \langle \phi_j | T_e + V_{eff}(r, R) | \phi_i \rangle \\ \Delta_{ji} &\equiv \langle \phi_j | \Delta(r, R) | \phi_i \rangle \ , \end{aligned} \quad (36)$$

respectively. For the diagonal elements of the density matrix a_{ji} this leads to

$$\dot{a}_{jj} = \sum_i b_{ji} + \sum_i \frac{2}{\hbar} \Re\left[a_{ji} \Delta_{ji}\right], \quad (37)$$

with $b_{ji} \equiv \frac{2}{\hbar} \Im\left[a_{ji} V_{ji}\right]$ and the density matrix elements defined as before. Note that for a normalised wave function Ψ the occupation probability a_{cc} for the "rest" is simply given by $a_{cc} \equiv 1 - \sum_j a_{jj}$, leading to

$$\dot{a}_{cc} = -\sum_j \dot{a}_{jj} = -\frac{2}{\hbar} \sum_{ij} \Re\left[a_{ji} \Delta_{ji}\right], \quad (38)$$

since $\sum_{ji} b_{ji} = 0$. The classically treated nuclear coordinates R obey formally the same Newtonian equation of motion as for the generalised surface hopping

$$\ddot{R} = \frac{-1}{M} \nabla \left[\frac{\langle \phi_{occ} | H_e | \phi_{occ} \rangle}{\langle \phi_{occ} | \phi_{occ} \rangle} \right], \tag{39}$$

where ϕ_{occ} is the currently occupied state. In order to determine both the classical and the quantum dynamics self-consistently, the equations (35) and (39) need to be integrated simultaneously while the currently occupied state is determined via the fewest switching algorithm. The probabilities P_{ji} for hops between the different potentials $\langle \psi_{occ} | H_e | \psi_{occ} \rangle \,/\, \langle \psi_{occ} | \psi_{occ} \rangle$ for the classical motion are for jumps between explicitly treated states

$$p_{ji} = \frac{\Delta t \, 2 \, \Im(a_{ij} V_{ij})}{\hbar a_{jj}}, \tag{40}$$

and the probability p_{jC} to go from state j to the collective state ϕ_C is given by

$$p_{jC} = \frac{-2\Delta t}{\hbar a_{jj}} \sum_i a_{ji} \Delta_{ji}. \tag{41}$$

As in the fewest switches algorithm, surface hopping switches between the states can occur at any point along the classical trajectories $R(t)$. Note that switches into the collective state occur only if the sum $\sum_i a_{ji}\Delta_{ji}$ is negative. We will also use this formalism to describe the excitation from the collective state into a particular electronic state j. For such a transition the sum in eq. (41) has to be positive, i.e. the sign of the optical potential has to be reversed. In order to simulated the excitation by a short laser pulse the optical potential needs to be time dependent which is a straight-forward generalisation.

This approach differs from the generalised surface hooping of the previous section in some points. First, we have introduced an optical potential in order to describe transitions to the collective state ψ. Furthermore we assume that the whole excess energy upon a transition to or from the continuum state is taken up by the substrate electrons, as it is usually done in the modelling of laser-induced desorption [17]. This means that upon a switch to the continuum state we just make a Franck-Condon transition, i.e. we transfer the molecule to the ground state potential with its kinetic energy preserved and perform ordinary Born-Oppenheimer molecular dynamics until the final fate of the molecule has been determined.

If just one electronically excited state is considered, then the equations become much simpler. According to eqs. (37) and (38), the de-excitation rate is directly given by

$$\dot{a}_{11} \;=\; -\dot{a}_{cc} \;=\; \dot{c}_1 c_1^* + c_1 \dot{c}_1^* = \frac{2 a_{11} \Delta(R)}{\hbar}. \tag{42}$$

In fact, for such a situation no electronic Schrödinger equation has to be integrated, leading to much shorter computation times.

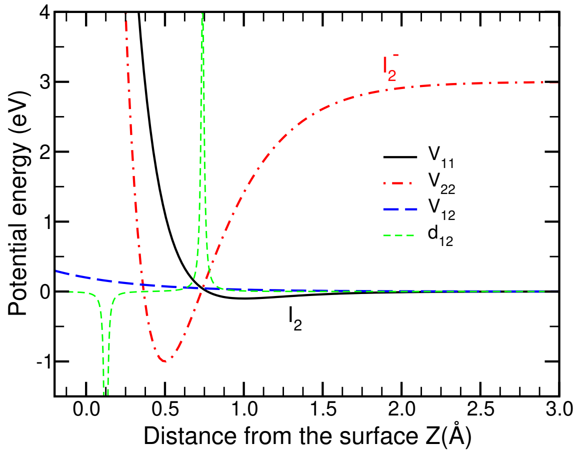

FIG. 2: One-dimensional two-state model potential for the ionization of I_2 in the scattering from diamond surfaces. V_{11} corresponds to the potential energy surface for the neutral molecule (solid line) and V_{22} to the potential for the charged molecule (dash-dotted line). V_{12} is the coupling between the two potentials (dashed line). The one-dimensional non-adiabatic coupling vector $\mathbf{d}_{12}$ (thin dashed line) is given in arbitrary units.

III. RESULTS AND DISCUSSION

A. Ionization probability in I_2 scattering from diamond

We will now review two recent applications of the mixed quantum-classical method to the description of reactions at surfaces with electronic transitions. The first example deals with the ionization probability in the scattering of I_2 from a diamond surface [19, 20]. Experimentally, above a threshold energy of about 3 eV a ionization probability strongly rising with increasing kinetic energy has been found [1]. At 10 eV kinetic energy of the incident I_2 molecules, the absolute I_2^- yield was 1%. In the absence of any *ab initio* total energy calculation for the I_2/diamond system, we modeled the interaction by an empirical potential. As a first step, we considered an one-dimensional two-state potential for I_2 and I_2^- interacting with diamond as a function of the molecular distance from the surface which is shown in Fig. 2. Both potentials were modeled as Morse potentials, the coupling between them was assumed to fall off exponentially with the distance from the surface. In addition, we have also included the non-adiabatic coupling vector d_{12} in Fig. 2. It is obvious that d_{12} is strongly localized at the curve crossings between the two diabatic curves.

The classical equations of motion eq. (14) together with the Schrödinger equation eq. (16) are numerically integrated with an Adams method using a variable time step [42]. The results thus obtained by the fewest-switches algorithm were compared to exact quantum simulations on the same potential for the one-dimensional situation. The quantum mechanical calculations of the

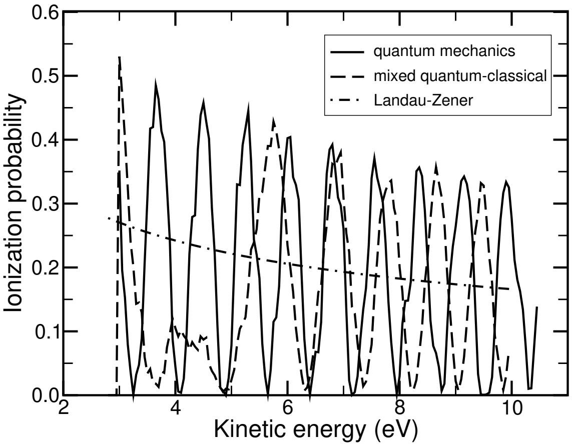

FIG. 3: Theoretical results of the ionization probability of I_2/diamond as a function of the incident kinetic energy of the molecule using an one-dimensional two-state potential. Thick solid line: quantum mechanical result; dashed line: semiclassical result within the adabatic representation; dash-dotted line: Landau-Zener approximation.

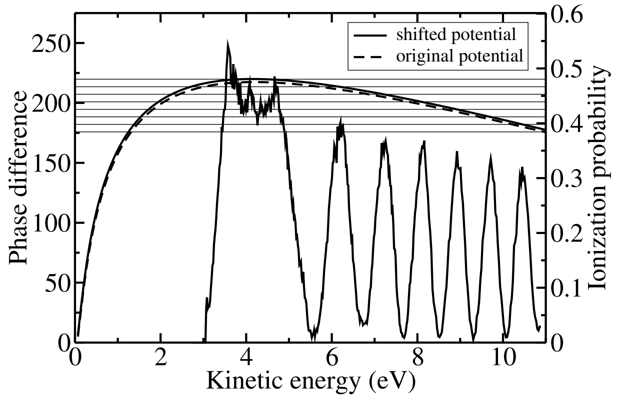

FIG. 4: Phase factor calculated according to eq. (46) for the original potential and for the excited state potential shifted by 25 meV. The horizontal lines indicate the condition for constructive interference. In addition, the ionization probability for the modified potential is shown.

ionization probability were performed by solving the time-independent Schrödinger equation within a coupled-channel scheme [11].

In Fig. 3, the ionization probability is plotted as a function of the incident kinetic energy. The thick solid line corresponds to the quantum mechanical results. The mixed quantum-classical results within the adiabatic representation were obtained by averaging over 1000 trajectories which leads to a statistical uncertainty of approximately 3%. In addition, we have included results according to the Landau-Zener approximation [19, 43] (dash-dotted line).

The quantum and mixed quantum-classical methods give an oscillatory behaviour of the ionization probability around nearly the same mean value which is approximately given by the Landau-Zener results. The scattered molecule can make transitions between the ground and excited state potential on the way to or from the surface. The oscillations, so-called Stückelberg oscillations, result from coherent interference between these two possible pathways. It is evident that the quantum and mixed quantum-classical results show the same amplitude of the Stückelberg oscillations, the phase, however, does not agree. This is not too surprising regarding that the semiclassical approximation breaks down at the classical turning points where the de Broglie wave length of the molecule becomes infinite.

In addition, in the mixed quantum-classical calculation one peak of the Stückelberg oscillations at approximately 4 eV is missing. The reason for the missing peak can be explained by analysing the time evolution of the density matrix elements. In our one-dimensional case with just two electronic states and a real non-adiabatic coupling vector the time evolution eq. (17) in the adiabatic representation can be expressed as a set of coupled differential equations

$$\begin{aligned} \dot{a}_{11} &= -2\dot{R}d_{12}\,\Re(a_{12}) \\ \dot{a}_{22} &= +2\dot{R}d_{12}\,\Re(a_{12}) \\ \dot{a}_{12} &= -\frac{ia_{12}}{\hbar}(V_{11}-V_{22}) + \dot{R}\,d_{12}(a_{11}-a_{22}) \\ \dot{a}_{21} &= +\frac{ia_{21}}{\hbar}(V_{11}-V_{22}) + \dot{R}\,d_{12}(a_{11}-a_{22}) \end{aligned} \quad (43)$$

Our simulations show, that the amplitude of the Stückelberg oszillations is related to the magnitude of the non-adiabatic coupling vector. But neither the frequency of the Stückelberg oscillations nor the missing peak are influenced by variations in the coupling vector. This can be easily understood: d_{12} is strongly localized at the curve crossing points of the diabatic potential curves and almost vanishes in the potential well. Hence all variations of the a_{ij} induced by d_{12} do not directly depend on the length of the path in the potential well. Furthermore, the effect of d_{12} on the a_{ij} almost cancels on the way to and from the surface due to the different sign of $\dot{R}$. Thus variations of d_{12} hardly change the phase of the a_{ij}, and consequently they do not alter the positions of the peaks.

On the other hand, the time evolution of a_{12} directly depends on the potential difference $\Delta V = V_{11} - V_{22}$ which assumes its maximum in the potential well. The difference $\Delta V(R(t))$ becomes a function of time along the trajectory $R(t)$ and thus depends implicitly on the kinetic energy. The second term on the right-hand side of the differential equation for a_{12} in (43) contributes only very little to the total phase difference, again because of the localized nature of d_{12}. This allows us to analyze the occurence of the Stückelberg oszillations in the limit of vanishing non-adiabatic coupling vector d_{12}. In this limit, the non-diagonal elements which describe the coherence evolve harmonically

$$\dot{a}_{12} = -\frac{i a_{12}}{\hbar} \Delta V \ . \tag{44}$$

The solution of this differential equation is

$$a_{12}(t) = a_{12}(t_0) \exp\left(-\frac{i}{\hbar} \int_{t_0}^{t} \Delta V(R(t'))dt' \right) \tag{45}$$

Thus the condition for constructive interference between the two pathways is given by

$$\int_{t_{up}}^{t_{down}} \Delta V(R(t'))dt' = 2\pi\hbar n, \, n \in Z \tag{46}$$

This integration has been performed numerically. In Fig. 4, we have plotted the phase factor eq. (46) as a function of the incident kinetic energy. The horizontal lines indicate the condition for constructive interference, i.e. they correspond to multiples of 2π. Constructive interference should occur at all points at which the phase factor crosses one of the horizontal lines. The phase factor for our original 1D two-state potential is shown by the dashed line. All peaks in Fig. 3 do indeed occur at the points where the phase factor fulfills the condition (46). Now one can understand why the peak at $E \approx 4$ eV is missing. There the phase difference shows its maximum, but it is just not sufficient for constructive interference.

This also means that if the potential diffence ΔV is slightly larger, constructive interference should occur at this energy. We checked this by just shifting the I_2^- potential down by 25 meV. We have also plotted the phase factor for the modified potential in Fig. 4 (solid line); in addition, we have included the ionization probability using the modified potential. Now the maximum of the phase factor lies slightly above a multiple of 2π. The condition for constructive interference is now approximately satisfied for a broad range of kinetic energies around 4 eV. Consequently, we get a broad peak in the ionization probability.

This analysis explains the occurence of the Stückelberg oscillations in the mixed quantum-classical calculations. However, it does not explain the difference between quantum and mixed quantum-classical calculations. Currently we still do fully understand this differences in the phase difference. It is obvious that the quantum phase difference between the two different paths to ionization is not correctly reproduced by the mixed quantum-classical calculations. At high energies above 8 eV, the distance between the peaks is correctly reproduced, but not the position. This means that there is a constant phase offset between quantum and mixed quantum-classical calculations which is most probably due to the behavior at the classical turning points, as already mentioned above. At lower kinetic energies, the distance between the peaks becomes larger in the mixed quantum-classical simulations since the phase factor approaches its maximum (see Fig. 4). In the quantum calculations, however, the peaks stay almost equidistant indicating that there is apparently no maximum in the phase difference.

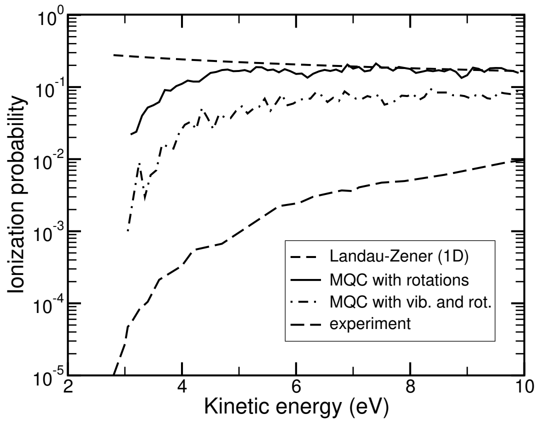

FIG. 5: Ionization probability of I_2/diamond as a function of the incident kinetic energy of the molecule. Solid line: 3D mixed quantum-classical (MQC) calculations including a surface oscillator and the molecular rotation; dash-dotted line: 4D MQC calculations taking additionally the molecular vibrations into account; long-dashed line: experimental results from ref. [1]. The 1D Landau-Zener results (short-dashed line) are plotted as a guide to the eye.

So far, the one-dimensional data showed no resemblance with the experimental results. However, any one-dimensional model describing a complex scattering event is often rather unrealistic. In order to make our model more realistic, we have taken into account more degrees of freedom. First of all, we added one surface oscillator coordinate in order to model energy transfer processes to the substrate. Furthermore, we included molecular rotations and vibrations [20]. Our still idealized four-dimensional model corresponds to the scattering of vibrating and rotating I_2 molecules on a flat vibrating surface.

As Fig. 5 shows, by taking into account more degrees of freedom, a significant suppression of the ionization probability is obtained, in particular at low kinetic energies. The reason for the suppression can be explained by a simple energy argument. The inclusion of more degrees of freedom in the scattering simulation causes an efficient energy transfer to these modes during the impulsive encounter. In our simulations up to several eV are transfered to the surface oscillator and the molecular rotations and vibrations. This energy is then missing for the transition over the ionization threshold of 3 eV. Thus we propose that it is not the electronic coupling *per se* that leads to the observed trend in the kinetic energy dependence of the ionization probability. It is rather the energy transfer to other degrees of freedom which causes the suppression of the ionization probability in particular for energies close to the ionization threshold. This explanation actually demonstrates the importance of high-dimensional simulations because it could not have been found in a one-dimensional model. It is also obvious from Fig. 5 that the Stückelberg oscillations are almost completely washed out in the higher-dimensional simulations. The multidimensionality of the charge transfer process leads to the loss of coherence. The remaining oscillations are due to the statistical uncertainty of ± 0.03 in the summation over the trajectories.

There are still large quantitative differences between the experiment and our 4D results, as Fig. 5 demonstrates. However, we have not tried to further adjust our potential parameters in order to achieve quantitative agreement with the experiment. Since our simulations are still performed within a limited geometry, there must still be room for the influence of other degrees of freedom in a more realistic simulation such as the lateral surface corrugation and the azimuthal anisotropy. Still, our calculations reproduce the observed qualitative dependence of the ionization probability in I_2/diamond scattering rather well and provide a physically reasonable explanation for this dependence. Of course we have to admit that this proposition is based on a model interaction potential. Hence we can not rule out other possible mechanisms.

B. Laser induced desorption of NO from NiO(100)

The photon-stimulated and the electron-stimulated desorption of molecules from surfaces has been intensively studied in the last decades [6]. In both kind of processes, the desorption is induced by electronic transitions (DIET). In Fig. 6, a DIET process is schematically shown. First the system is excited in a Franck-Condon transition by, e.g., a laser pulse. This pulse may directly excite the adsorbate, but most probably first the substrate becomes electronically excited with the creation of hot electrons. On the excited state potential, the adsorbate is no longer at a minimum position; therefore it becomes accelerated. After a certain lifetime the adsorbate returns to its electronic ground state in a second Franck-Condon transition, i.e. without changing its velocity. Often this is depicted by a transition down to the ground state potential. However, the excess energy of this transition has to be taken up by the substrate which then becomes electronically excited through, e.g, the population of electron-hole pairs. Hence this transition should be rather regarded as occuring at a curve crossing between the excited adsorbate state and the electronic adsorbate ground state together with a substrate excitation. In Fig. 6, we have assumed that the excitation of delocalized electron-hole pairs in the substrate does not modify the adsorbate electronic ground state potential.

Thus for a realistic modelling of a DIET process, the quasi-continuum of substrate excitations has to be taken into account appropriately. Of course it is impossible to explicitly include all substrate excitations. Therefore we take the substrate excitations into account through a optical potential, as described by eqs. (33) and (34).

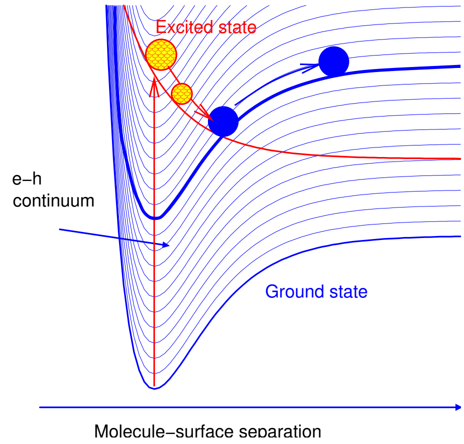

FIG. 6: Schematic drawing of a desorption process induced by electronic transitions. The electronic ground state adsorbate potential together with the quasi-continuum of substrate excitations and a excited state adsorbate potential are shown.

Note that such an approach in the modelling of DIET processes has been used before [38, 39, 44]. In detail, in our mixed quantum-classical implementation we describe the laser induced desorption as follows (see Fig. 6). We start with the mixed quantum-classical simulation after the first Franck-Condon transition on the excited state surfaces. The norm of the wave function decreases due to the presence of the optical potential $\Delta(E)$ which is illustrated by the reduced diameter of the circle representing the particle on the excited state potential in Fig. 6. By comparing the norm of the wave function with a random number we decide whether the second Franck-Condon transition back to the molecular ground state occurs with the excess energy taken up by the substrate. Finally, molecular dynamics simulations are performed on the adiabatic ground state, i.e. without any optical potential, in order to determine the desorption distributions.

As a first application we have used this scheme to investigate the laser induced desorption of NO from a NiO(100) surface. The experimentally observed desorption cross section in this system is several orders of magnitude larger than that from metal substrates (10^{-17}cm^2 vs 10^{-21}cm^2 [45]). One of the most interesting experimental observations is the measured bimodality in the velcocity distribution of the desorbing NO molecules. This system has already been addressed by theoretical studies [23, 46–49]. A two-dimensional potential energy surface for the ground and a charge transfer state as a function of the NO center of mass distance from the surface Z and the polar orientation θ of the molecule was determined by quantum chemical calculations. Based on this potential, jumping wave-packet simulations of the laser induced simulations were performed [23]. In these calculations, the observed bimodality in the velocity distribution could be reproduced qualitatively. The simulations suggested that the bimodality is a consequence of

	2D	3D	6D	7D
P_{des} (%)	4.84	3.63	4.74	4.02
P_{early} (%)	2.93	0.32	2.53	0.32
E_{rot} (K)	770	366	883	395

TABLE I: Desorption probabilities and mean rotational energies according to the 2D, 3D, 6D and 7D calculations. Early means desorption within the first 1.2 picoseconds.

a bifurcation of the wave-packet due to the topology of the excited state potential energy surface.

We have used the parametrized version of the *ab initio* potential for NO/NiO(100) as the basis of mixed quantum-classical simulations of the laser-induced desorption of NO from NiO(100). As a first step, we determined the desorption probabilities and distributions within the same two-dimensional setup as used in the wave-packet calculations. Using the same numerical parameters, we obtained good agreement between the wave-packet and the mixed quantum-classical results [21, 22]. However, we found that there are two kinds of desorbing trajectories, those desorbing within the first 1.2 picoseconds, which we will call early, and a long trail of late desorbing trajectories. On the ground state the molecules hit the repulsive potential wall and either scatter directly into the vacuum, giving rise to the early desorbing species, or start to rotate in front of the surface thus becoming dynamically trapped [16, 50–52] and leading to the late species.

The wave-packet results were obtained by propagating in the ground state until the desorption yield seemingly saturated, so that only the early channel was captured. In Table I, we have listed the main results with respect to the total desorption probability P_{des} and the rotational temperature of desorbing molecules according to the mixed-quantum calculations. P_{early} denotes the fraction of molecules desorbing in the early channel.

For a more realistic modelling of the desorption process we extended the *ab initio* two dimensional potentials to in total seven dimensions by taking into account all six molecular degrees of freedom plus one surface oscillator coordinate in order to allow for energy transfer between molecule and substrate. In the absence of any *ab initio* results we were required to use a model potential for the additional degrees of freedom. Thus the particular choice of the parameters has to be considered as an educated guess. We like to point out, however, that the qualitative results we obtained did not depend very sensitively on the particular choice of parameters.

Going from 2D to 6D, i.e. including the remaining molecular degrees of freedom in the simulations, has only a small influence on the desorption dynamics, as Table I shows. The same is also true for the transition from 3D to 7D. However, including recoil processes of the substrate, by coupling the motion of the adsorbate molecule to a surface oscillator, changes the outcome of the trajectory calculations significantly. While the total desorption

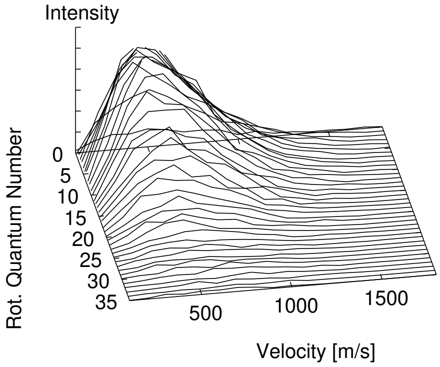

FIG. 7: Velocity distributions as a function of the rotational state according to the seven-dimensional mixed quantum-classical calculations.

probability is only reduced by about 1%, the effect on the early desorption channel is really significant: It is reduced by a factor of eight (see Table I). But the most dramatic effect of the surface oscillator is on the rotational momentum distribution. While in the 2D calculations we obtain a double peaked structure with a large probability for high rotational quantum numbers, the inclusion of the surface oscillator causes the suppression of the peak at high J. The shape of the distribution is now similar to that of the late molecules in the rigid surface case. This is leading to a greatly reduced mean rotational energy of the desorbing molecules, 366 K and 395 K for 3D and 7D calculations, respectively, instead of 770 K for the 2D and 883 K for the 6D calculations. These reduced rotational temperatures are in fact in much better agreement with experiment [45].

As far as the velocity distribution in desorption is concerned, however, the agreement between theory and experiment is greatly reduced if the late desorption channel and the surface oscillator are taken into account. In Fig. 7, we have plotted the momentum distribution according to the 7D calculations. There is no indication of any bimodal velocity distribution which was found in the experiment [45] and which was also reproduced in the wave-packet calculations [23]. Note that apart from an overall scaling due to the reduced desorption probability the shapes of the velocity distributions summed over all rotational momenta are almost identical for all dimensionalities used.

These findings do not necessarily imply that the conclusions of Ref. [23] with respect to the origins of the bimodality in the velocity distribution are no longer valid. It might well be that the explanation in terms of a bifurcation of the wave-packet is still correct. However, in the simulations only one excited charge transfer state potential out of a great number of charge transfer states [46] has been chosen. Possibly more than one excited state might be involved in the desorption process. Furthermore, the extension of the two-dimensional *ab initio* po-

γ [fs^{-1}]	0.0	0.0002	0.0005	0.001	0.002
τ_D [ps]	∞	10.0	4.0	2.0	1.0
P_{des} [%]	4.43	1.46	0.73	0.27	0.07

TABLE II: Values used for the friction constant γ and corresponding decay times τ_D and desorption probabilities.

tential to seven dimensions using a physically reasonable model potential could not be realistic enough. This will be checked by mapping out higher-dimensional potential energy surfaces through quantum chemical calculations. Finally, the consideration of a spatially varying transition probability could lead to a better agreement between theory and experiment. If the deexcitation mainly occurs at specific configurations of the adsorbate, this can have a strong effect on the desorption dynamics.

To investigate the possible effect of dissipation at the surface on the desorption dynamics we added a frictional force term $-m\gamma\dot{s}$ to the surface oscillator in the full dimensional model, i.e. if $\ddot{s} = F_s(R)$ was the original equation of motion with the force $F_s(R)$ and R standing for all the coordinates, the new equation of motion is given by

$$\ddot{s} = F_s(R) - m\gamma\dot{s}. \qquad (47)$$

If we are not in the aperiodic limit, i.e. if $\gamma < 2\omega$ where ω is the oscillator frequency, the oscillation amplitudes of a free damped oscillator decrease with time as $\exp(-\gamma t/2)$ and the corresponding decay time τ_D is given by $\tau_D = 2/\gamma$. The values used for γ and the corresponding decay times τ_D are shown in table II. We used decay times between 1 ps and 10 ps as we would expect them for phonon mediated energy dissipation. We see that already a relatively small friction causes a considerable drop in the desorption probability from 4.4 percent down to 1.5 %. A closer analysis shows that almost all the dissipation takes place while the molecule is in its ground state and only the time during which desorption still occurs is shortened by the friction. Without friction, there is a long trail of molecules desorbing at very large times, which contribute a substantial amount to the total desorption probability. This tail is cut off by the dissipative effects and thus lowering the desorption probability.

The effect of the friction on the momentum distribution and the vibrational, oscillator and rotational state occupation probabilities of the desorbing molecules is negligible, apart from an overall scaling due to the reduced desorption probability. Most trajectories that do desorb leave the surface at times usually smaller than the corresponding decay time τ_D of the oscillator. Thus the amount of energy lost is rather small and thus the final occupation probabilities are almost unaffected. Note that this is true for all frictional constants used.

IV. CONCLUSIONS

We have implemented a mixed quantum-classical surface hopping scheme for the simulation of electronically non-adiabatic processes at surfaces. In this method, the nuclear motion is described classically while the electrons are treated quantum mechanically. Still the feedback between nuclei and electrons is fully taken into account. In contrast to a quantum treatment the computational efficiency of our method allows a multi-dimensional treatment. We have applied this method to the ionization of I_2 in the scattering from a diamond surface and to the laser-induced desorption of NO from NiO(100) using a previously determined *ab initio* potential energy surface. By comparing our method to low-dimensional quantum calculations on exactly the same potential energy surfaces we verified that it is indeed justified to neglect quantum effects in the nuclear motion.

Our mixed-quantum classical method is computationally very efficient. This has allowed us to extend the simulations to longer time scales and higher dimensionalities. Our high-dimensional simulations demonstrate the importance of the multi-dimensionality in the reaction dynamics. In the system I_2/diamond, our calculations suggest that the dependence of the ionization probability on the kinetic energy is not determined by the electronic coupling *per se*, but by the energy transfer to other degrees of freedom during the scattering process. For the laser-induced desorption of NO/NiO(100) we find that the bimodality in the velocity distribution of desorbing molecules obtained in low-dimensional simulations vanishes if in particular surface recoil processes are taken into account. This indicates that more than one excited state might be involved in the desorption process.

[1] Danon, A.; Amirav, A. *Phys. Rev. Lett.* **1988**, *61*, 2961.

[2] Greber, T. *Surf. Sci. Rep.* **1997**, *28*, 3.

[3] Gergen, B.; Nienhaus, H.; Weinberg, W. H.; McFarland, E. W. *Science* **2001**, *294*, 2521.

[4] Tolk, N. H., Traum, M. M., Tully, J. C., Madey, T. E., Eds.; *Desorption induced by Electronic Transitions DIET I*, Vol. 24 of *Springer Series in Chemical Physics.* Springer, **1983**.

[5] Brenig, W., Menzel, D., Eds.; *Desorption Induced by Electronic Transitions DIET II*, Vol. 4 of *Springer Series in Surface Sciences*. Springer, **1984**.

[6] Zimmermann, F. M.; Ho, W. *Surf. Sci. Rep.* **1995**, *22*, 127.

[7] Eichhorn, G.; Richter, M.; Al-Shamery, K.; Zacharias, H. *J. Chem. Phys.* **1999**, *111*, 386–397.

[8] Bonn, M.; Kleyn, A. W.; Kroes, G. J. *Surf. Sci.* **2002**, *500*, 475.

[9] Bonn, M.; Funk, S.; Hess, C.; Denzler, D. N.; Stampfl, C.; Scheffler, M.; Wolf, M.; Ertl, G. *Science* **1999**, *285*, 1042.

[10] Petek, H.; Weida, M. J.; Nagano, H.; Ogawa, S. *Science* **2000**, *288*, 1402.
[11] Brenig, W.; Brunner, T.; Groß, A.; Russ, R. *Z. Phys. B* **1993**, *93*, 91.
[12] Groß, A. *Surf. Sci. Rep.* **1998**, *32*, 291.
[13] Kroes, G.-J. *Prog. Surf. Sci.* **1999**, *60*, 1.
[14] Groß, A. *Surf. Sci.* **2002**, *500*, 347.
[15] Brenig, W.; Hilf, M. F. *J. Phys. Condens. Mat.* **2001**, *13*, R61.
[16] Groß, A.; Eichler, A.; Hafner, J.; Mehl, M. J.; Papaconstantopoulos, D. A. *Surf. Sci.* **2003**, *539*, L542.
[17] Guo, H.; Saalfrank, P.; Seideman, T. *Prog. Surf. Sci.* **1999**, *62*, 239.
[18] Tully, J. C. *J. Chem. Phys.* **1990**, *93*, 1061–1071.
[19] Bach, C.; Groß, A. *Faraday Diss.* **2000**, *117*, 99.
[20] Bach, C.; Groß, A. *J. Chem. Phys.* **2001**, *114*, 6396.
[21] Bach, C.; Klüner, T.; Groß, A. *Chem. Phys. Lett.* **2003**, *376*, 424.
[22] Bach, C.; Klüner, T.; Groß, A. *Appl. Phys. A* **2004**, *78*, 231.
[23] Klüner, T.; Freund, H.-J.; Staemmler, V.; Kosloff, R. *Phys. Rev. Lett.* **1998**, *80*, 5208.
[24] Tully, J. C. *Faraday Discussions* **1998**, *110*, 407–419.
[25] Tully, J. C. *Modern Methods for Multidimensional Dynamics Computations in Chemistry;* ed. by D. L. Thompson, World Scientific: Singapore, 1998, ch. 2.
[26] Hammes-Schiffer, S.; Tully, J. C. *J. Chem. Phys.* **1994**, *101*, 4657–4667.
[27] Hammes-Schiffer, S.; Morelli, J. April **1997**, *269*, 161–170.
[28] Tully, J. C.; Preston, R. K. July **1971**, *55*, 562–572.
[29] Herman, M. F. *J. Chem. Phys.* **1983**, *81*, 754–763.
[30] Herman, M. F. *J. Chem. Phys.* **1983**, *81*, 764–774.
[31] Herman, M. F. *J. Chem. Phys.* **1985**, *82*, 3666–3673.
[32] Pechukas, P. *Phys. Rev.* **1969**, *181*, 166–174.
[33] Pechukas, P. *Phys. Rev.* **1969**, *181*, 174–185.
[34] Herman, M. F. *J. Chem. Phys.* **1982**, *76*, 2949–2958.
[35] Müller, U.; Stock, G. *J. Chem. Phys.* **1997**, *107*, 6230–6245.
[36] Coker, D.; Xiao, L. *J. Chem. Phys.* **1995**, *102*, 496–510.
[37] Sholl, D. S.; Tully, J. C. *J. Chem. Phys.* **1998**, *109*, 7702–7710.
[38] Brenig, W. *Z. Phys. B* **1976**, *23*, 361–368.
[39] Saalfrank, P. *Chem. Phys.* **1995**, *193*, 119–139.
[40] Newton, R. G. *Scattering Theory of Waves and Particles;* McGraw-Hill, 1966.
[41] Brako, R.; Newns, D. M. *Rep. Prog. Phys.* **1989**, *52*, 655.
[42] Gautschi, W. *Numerical Analysis, an Introduction;* Birkhäser, 1997.
[43] Landau, L. D.; Lifshitz, E. M. *Quantum Mechanics, Nonrelativistic Theory;* Pergamon Press, 1958.
[44] Menzel, D.; Gomer, R. December **1964**, *41*, 3311–3328.
[45] Mull, T.; Baumeister, B.; Menges, M.; Freund, H.-J.; D.Weide.; Fischer, C.; Andersen, P. *J. Chem. Phys.* **1992**, *96*, 7108–7116.
[46] Klüner, T.; Freund, H.-J.; Freitag, J.; Staemmler, V. *J. Chem. Phys.* **1996**, *104*, 10030–10040.
[47] Klüner, T.; Freund, H.-J.; Freitag, J.; Staemmler, V. *J. Mol. Catal. A* **1997**, *119*, 155.
[48] Koch, C. P.; Klüner, T.; Freund, H.-J.; Kosloff, R. *Phys. Rev. Lett.* **2003**, *90*, 117601.
[49] Koch, C. P.; Klüner, T.; Freund, H.-J.; Kosloff, R. *J. Chem. Phys.* **2003**, *119*, 1750.
[50] Groß, A.; Scheffler, M. *J. Vac. Sci. Technol. A* **1997**, *15*, 1624.
[51] Busnengo, H. F.; Dong, W.; Salin, A. *Chem. Phys. Lett.* **2000**, *320*, 328.
[52] Crespos, C.; Busnengo, H. F.; Dong, W.; Salin, A. *J. Chem. Phys.* **2001**, *114*, 10954.